Cellular and Molecular Life Sciences (2025) 82:66
https://doi.org/10.1007/s00018-024-05535-2

ORIGINAL ARTICLE

Ebastine-mediated destabilization of E3 ligase MKRN1 protects against metabolic dysfunction-associated steatohepatitis

Seungyeon Kim[1] · Hyun-Ji Han[1] · Hyunjin Rho[1] · Subin Kang[1] · Sulagna Mukherjee[2] · Jiwoo Kim[3] · Doyoun Kim[3,4,5] · Hyuk Wan Ko[1,7] · Sang Min Lim[5] · Seung-Soon Im[2] · Joon-Yong Chung[6] · Jaewhan Song[1,7]

Received: 20 June 2024 / Revised: 8 November 2024 / Accepted: 29 November 2024

Abstract

Metabolic dysfunction-associated steatotic liver disease (MASLD) is a chronic condition encompassing metabolic dysfunction-associated steatotic liver (MASL) and metabolic dysfunction-associated steatohepatitis (MASH), which can progress to fibrosis, cirrhosis, or hepatocellular carcinoma (HCC). The heterogeneous and complex nature of MASLD complicates optimal drug development. Ebastine, an antihistamine, exhibits antitumor activity in various types of cancer. However, its effects on MASH remain unexplored. In the present study, we identified ebastine as a potential treatment for MASH. Our results indicated that ebastine acts as a novel MKRN1 inhibitor by promoting MKRN1 destabilization through self-ubiquitination, leading to AMP-activated protein kinase (AMPK) activation. Ebastine appeared to bind to the C-terminal domain of MKRN1, particularly at residues R298 and K360. Notably, *Mkrn1* knockout (KO) mice demonstrated resistance to MASH, including obesity, steatosis, inflammation, and fibrosis under high-fat-high-fructose diet (HFHFD) conditions. Additionally, liver-specific *Mkrn1* knockdown using AAV8 alleviated MASH symptoms in HFHFD-fed mice, implicating MKRN1 as a potential therapeutic target. Consistent with these findings, treatment with ebastine significantly reduced the risk of MASH in HFHFD-fed mice, with a decrease in MKRN1 expression and an increase in AMPK activity. Our study suggests that ebastine binds to MKRN1, promoting its destabilization and subsequent degradation by stimulating its ubiquitination. This enhances AMPK stability and activity, suppressing lipid accumulation, inflammation, and fibrosis. Moreover, the knockout of *Mkrn1* mice decreased the risk of MASH, suggesting that ebastine could be a promising therapeutic agent for the treatment of MASH.

Keywords AMP-activated protein kinase (AMPK) · MKRN1 · Ebastine · Metabolic dysfunction-associated steatohepatitis (MASH)

✉ Jaewhan Song
jso678@yonsei.ac.kr

[1] Department of Biochemistry, College of Life Science and Biotechnology, Yonsei University, Seoul 03722, Republic of Korea

[2] Department of Physiology, Keimyung University School of Medicine, Daegu 42601, Republic of Korea

[3] Therapeutics & Biotechnology Division, Drug Discovery Platform Research Center, Korea Research Institute of Chemical Technology (KRICT), Daejeon 34114, Republic of Korea

[4] Medicinal Chemistry and Pharmacology, Korea University of Science and Technology (UST), Daejeon 34113, Republic of Korea

[5] Brain Science Institute, Korea Institute of Science and Technology, Seoul 07292, Republic of Korea

[6] Molecular Imaging Branch, Center for Cancer Research, National Cancer Institute, National Institutes of Health, Bethesda, MD 20892, USA

[7] Department of Biochemistry, College of Life Science and Technology, Institute for Bio-medical Convergence Science and Technology, Yonsei University, Seoul, Republic of Korea

Published online: 31 January 2025

Introduction

Metabolic dysfunction-associated steatotic liver disease (MASLD) refers to fatty liver disease in individuals who exhibit at least one cardiometabolic risk factor but lack a history of excessive alcohol consumption [1–3]. MASLD symptoms can be typically divided into metabolic dysfunction-associated steatotic liver (MASL) and metabolic dysfunction-associated steatohepatitis (MASH), depending on disease severity [4, 5]. MASH, a severe form of MASLD, is usually diagnosed when there is more than 5% hepatic steatosis and inflammation, with hepatocellular injury in the presence or absence of fibrosis [6, 7]. While the presence of fibrosis is not a prerequisite for diagnosing MASH, fibrosis is observed in over 80% of the livers of patients with this disease who can be categorized by their stage of fibrosis. Patients with advanced MASH are at high risk of developing decompensated liver cirrhosis, end-stage liver disease, and hepatocellular carcinoma (HCC) [5]. Consequently, MASH imposes a great clinical and economic burden on healthcare systems worldwide, resulting in hepatic and extrahepatic comorbidities and the need for liver transplants. Furthermore, the incidence of MASLD has increased owing to over-nutrition and sedentary lifestyles, making it one of the most common diseases worldwide. A recent meta-analysis indicated that the global prevalence of MASLD among adults was approximately 25%. Among these patients, approximately 25% develop MASH and develop comorbidities, with approximately 2% succumbing to MASLD liver-related complications [8, 9]. As no approved drugs for the treatment of MASL or MASH are available, there is an urgent medical need to identify therapeutic targets and drugs to treat these diseases [10, 11]. Moreover, while Rezdiffra (resmetirom), developed by Madrigal Pharmaceuticals, resulted in approximately 30% improvement in liver scarring and MASH resolution and has been recently approved by the FDA, there remains an urgent medical need to identify more therapeutic targets and drugs to treat these diseases [10, 11].

One of the therapeutic targets for MASLD is AMP-dependent protein kinase (AMPK), which plays an important role in regulating cellular energy status under various nutritional conditions [12, 13]. Activation of AMPK under low-energy conditions reprograms cellular metabolism towards catabolic processes and restores the ATP balance while deactivating anabolic pathways [14]. AMPK is considered the central mediator of metabolic stress at the cellular and systemic levels, balancing energy homeostasis via lipid and glucose metabolism, autophagy, mTORC pathways, and mitochondrial biogenesis [14, 15]. AMPK is a phylogenetically conserved serine/threonine protein kinase consisting of one α catalytic subunit and two β and γ regulatory subunits. Its activation is initiated by the interaction of its γ subunit with AMP, which induces the phosphorylation of the α catalytic subunit on Thr172 by upstream kinases including LKB1, CaMKKIIβ, and TAK1 [16]. AMPK activity can also be influenced by different distributions and combinations of α, β, and γ isoforms (α1, α2, β1, β2, γ1, γ2, γ3) in different tissues. Given its role in major metabolic pathways controlling whole-body glucose and lipid homeostasis, hepatic AMPK is considered a major therapeutic target for metabolic disorders such as type 2 diabetes and MASLD [12, 17]. Pan-AMPK activators, such as metformin, A-76966, AICAR, O304, MK8722, PF-739, and salicylate, improve insulin resistance and hyperglycemia [18–21]. Drugs indirectly activating AMPK, such as metformin, statins, ezetimibe, and sorafenib, can ameliorate liver metabolic disorders including MASLD and diabetes [22–25]. In vivo studies using transgenic or knockout (KO) mice have indicated that AMPK protects against hepatic steatosis and hepatocyte injury [26–29]. Although several AMPK activators, such as metformin and PXL770, are being clinically tested for MASH treatment, no approved AMPK target drugs are currently available [30]. Several animal model reports indicate that while AMPK functions as a major modulator of energy homeostasis, its stability and function are affected by post-translational modulators, subsequently influencing related metabolic phenomena. For example, E3 ligases, such as CHIP, CRBN, and MKRN1, as well as the deubiquitinase USP10, play a critical role in regulating AMPK stability and activity through post-translational modifications (PTMs), and consequently, impact metabolic processes in animal models [31–34]. Among these modulators, MKRN1 targets AMPK in ubiquitin-dependent proteasomal degradation. Notably, *Mkrn1* whole-body KO mouse models were reported to be protected against high-fat diet (HFD)-induced obesity and diabetes through the stabilization and activation of AMPK in both adipose and hepatic tissues [34]. However, the role of MKRN1 in regulating hepatic inflammation or fibrosis during MASH remains unclear.

Recently, several antihistamines have been discovered to exhibit antitumor effects in various types of cancer, expanding beyond their traditional role in treating allergies [35–37]. Ebastine, an antihistamine belonging to the piperidine derivative class of small molecules, exhibits antitumor activity in various types of cancer [35, 38, 39]. However, research has not yet explored the full potential of ebastine in regulating MASH. In the present study, we investigated the therapeutic potential of ebastine in MASH and demonstrated that ebastine induced ubiquitin–proteasome-dependent destabilization of MKRN1 with concomitant stabilization of AMPK, which might alleviate MASH symptoms and fibrosis in mice fed a HFHFD via intraperitoneal injection. These results

suggest the potential of ebastine in targeting MKRN1 for MASH treatment.

Results

Depletion of *Mkrn1* suppresses HFHFD-induced MASH

We fed mice a HFHFD to establish a MASH model. When mice were fed a HFHFD for 20 or 30 weeks, the size and weights of mice lacking *Mkrn1* ($MK1^{-/-}$) were significantly lower than those of wild-type (WT) mice under the same average food and fructose water intake conditions (Fig. S1A–I). Similarly, the adipocyte areas of brown adipose tissue (BAT) and white adipose tissue (WAT) were smaller in $MK1^{-/-}$ mice than in WT mice (Fig. S1J–M). Moreover, the liver weights of $MK1^{-/-}$ mice were lower than those of WT mice (Fig. 1A, B). Histological analyses revealed the occurrence of hepatocellular ballooning, inflammation, or Mallory-Denk Bodies with lipid droplet accumulation in the hepatocytes of WT mouse livers. However, these phenomena were absent in $MK1^{-/-}$ mice (Fig. 1C, D). Furthermore, collagen secretion and macrophages were detected in WT mice using Sirius red and f4/80 staining, respectively. As the f4/80 markers are mostly detected in Kupffer cells, the staining primarily reflects Kupffer cell involvement in the inflammatory response [40, 41]. However, $MK1^{-/-}$ mice were protected against fibrosis and inflammation, as evidenced by the lack of positivity for either stain (Fig. 1E, F). These observations were further confirmed via quantitative real-time PCR (qRT-PCR), revealing decreased expression of fibrotic and inflammatory genes in the livers of $MK1^{-/-}$ mice compared to WT mice (Figs. 1G and S2A–D). Accordingly, the serum levels of aspartate aminotransferase (AST), alanine aminotransferase (ALT), triglycerides (TGs), and cholesterol were significantly lower in $MK1^{-/-}$ mice than in WT mice (Fig. 1H, I). Moreover, the stabilization and activation of AMPKα were also enhanced in the livers of $MK1^{-/-}$ mice compared to those in WT mice, leading to the suppression of its downstream target, acetyl-CoA carboxylase (ACC), through increased ACC phosphorylation (Fig. 1J, K) [13, 14, 16]. Quantitative analyses showed that the pAMPK/total AMPK ratio in the liver was similar between WT and $MK1^{-/-}$ mice, indicating that the increased levels of pAMPK were likely due to higher levels of total AMPK stabilized by MKRN1 depletion. These findings suggest that MKRN1 targets total AMPK, instead of pAMPK, for degradation (Fig. S2E, F). Finally, no significant changes in glycogen accumulation in mice fed a HFHFD were observed (Fig. S2G). Overall, *Mkrn1* depletion in mice conferred hepatic protection against HFHFD-induced MASH by promoting AMPK activity.

Protective effect of MASH via *Mkrn1* depletion is nullified by simultaneous knockout of *Ampkα2*

As the results indicated that *Mkrn1* depletion promoted the stabilization and activation of AMPK in mouse liver, under metabolic stress, and alleviated MASH, we further investigated the genetic association between AMPK and MKRN1. Considering prior reports indicating that metabolic stress significantly reduces AMPKα2 expression without affecting AMPKα1, we generated double knockout (DKO) mice in which *Ampkα2* and *Mkrn1* were simultaneously depleted to clearly elucidate the regulatory relationship between MKRN1 and AMPKα2 under metabolic stress (Fig. S3A–C) [42]. When WT, $MK1^{-/-}$, or DKO mice were fed a HFHFD, $MK1^{-/-}$ mice exhibited lower body weights during metabolic stress, whereas DKO mice had body weights similar to those of the WT mice under the same average food and fructose water intake conditions (Figs. 2A and S3D–F). Similarly, DKO mice exhibited enlarged liver sizes and weights comparable to those of WT mice. In contrast, $MK1^{-/-}$ mice had smaller liver sizes and weights, as well as reduced adipocyte sizes, compared to WT (Figs. 2B, C, and S3G). Consistent with these data, the anti-obesity, anti-fibrotic, and anti-inflammatory effects of $MK1^{-/-}$ mice were completely nullified in the DKO mice in terms of steatosis, fibrosis, and inflammation occurrences, respectively. These patterns were similar to those observed in WT mice (Fig. 2D–J). Serum AST, ALT, TG, and cholesterol levels were decreased in $MK1^{-/-}$ mice and increased in DKO mice, similarly to WT mice (Fig. 2K, L). Moreover, AMPK stabilization and activation were significantly increased in the livers of $MK1^{-/-}$ mice compared to those in the livers of WT or DKO mice (Fig. S3H). Finally, no significant changes were observed in glycogen accumulation (Fig. S3I). These observations provide genetic evidence of a negative correlation between AMPKα2 and MKRN1 and indicate that the suppression of MKRN1 activity could enable AMPKα2 to inhibit MASH.

Liver-specific depletion of *Mkrn1* suppresses HFHFD-induced MASH

To analyze the acute effects of *Mkrn1* depletion on MASH, we used an AAV8 system expressing *Mkrn1* shRNA to knockdown *Mkrn1* in the liver. Mice fed a HFHFD for 8 or 10 weeks were injected with AAV8 sh*Mkrn1* and subsequently fed a HFHFD for 12 or 20 weeks, respectively (Fig. 3A, B). The infection of the liver by AAV8 was confirmed via GFP detection of the AAV8 marker (Fig. S4A). Decreased levels of *Mkrn1* were further confirmed by the detecting both mRNA and protein expression levels in the liver (Figs. 3C and S4B). Upon expression of AAV8 sh*MKRN1*, no notable differences were observed in the weight of

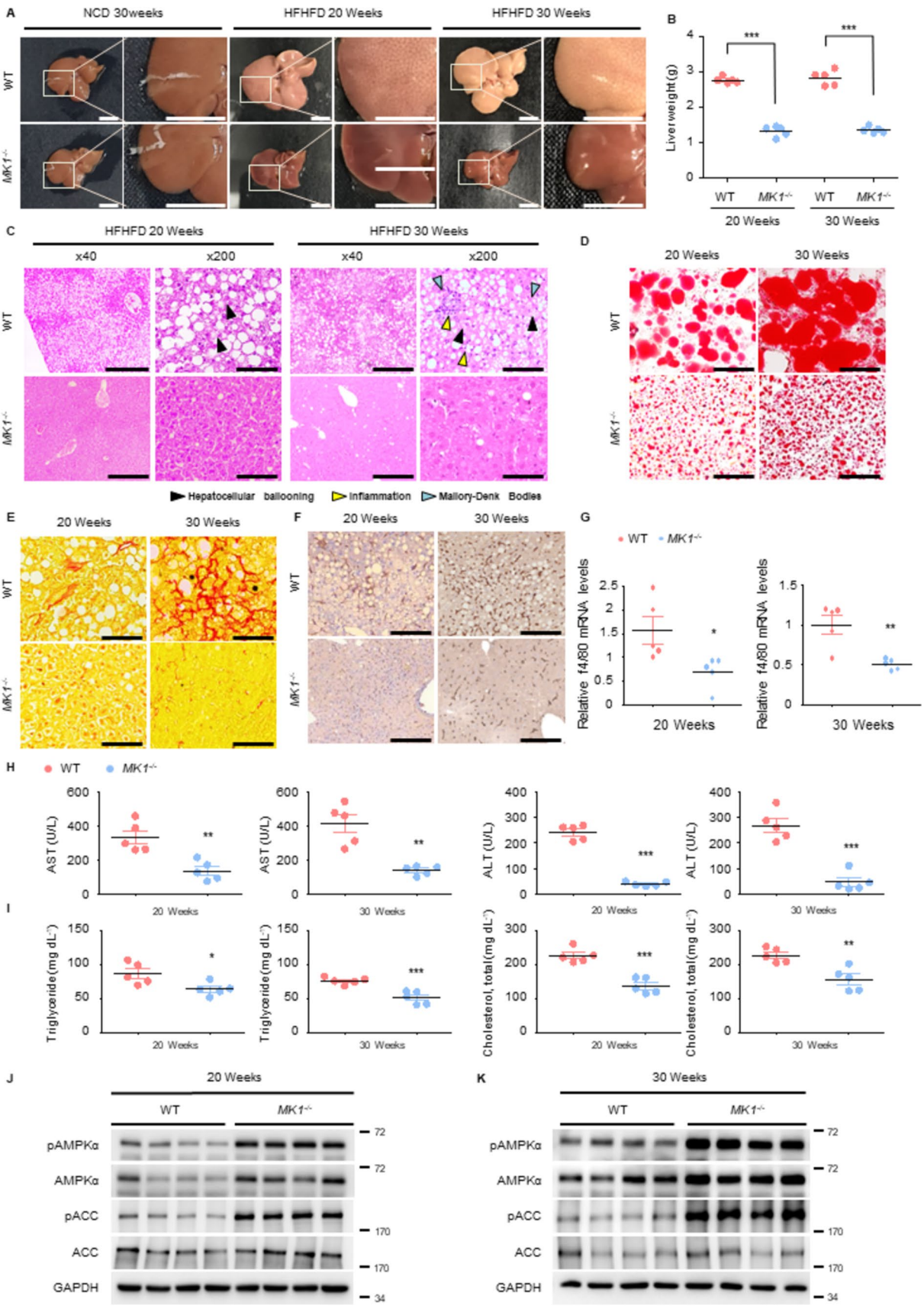
A
NCD 30weeks
HFHFD 20 Weeks
HFHFD 30 Weeks
WT
MK1-/-
B
Liver weight (g)
WT
MK1-/-
20 Weeks
30 Weeks
C
HFHFD 20 Weeks
HFHFD 30 Weeks
x40
x200
Hepatocellular ballooning
Inflammation
Mallory-Denk Bodies
D
20 Weeks
30 Weeks
E
F
G
Relative f4/80 mRNA levels
H
AST (U/L)
ALT (U/L)
I
Triglyceride (mg dL-1)
Cholesterol, total (mg dL-1)
J
K
pAMPKα
AMPKα
pACC
ACC
GAPDH

◂**Fig. 1** MASH induced by HFHFD was alleviated in *MK1*$^{-/-}$ mice. **A** Representative livers of WT and *MK1*$^{-/-}$ mice fed NCD or HFHFD (Scale bar = 1 cm). **B** Liver weights of WT or *MK1*$^{-/-}$ mice fed NCD or HFHFD (n = 5 mice per group). **C** H&E staining of the livers (Scale bars; × 40 = 250 μm and × 200 = 25 μm). Black, yellow, and blue arrowheads indicate hepatocellular ballooning, inflammation, and Mallory-Denk bodies, respectively. **D** Representative images of Oil Red O staining of the livers. (Scale bar = 25 μm). **E** Representative images of Sirius red staining of the livers. (Scale bar = 25 μm). **F** Representative images of f4/80 staining of the livers. (Scale bar = 100 μm). **G** mRNA expression levels of f4/80 in the livers of mice fed HFHFD for 20 (left) or 30 (right) weeks (n = 5 mice per group). **H** AST and ALT serum levels (n = 5 mice per group). **I** Plasma concentrations of TG and cholesterol (n = 5 mice per group). **J**, **K** Lysates of the liver tissues were analyzed by western blotting. Two-tailed Student's *t*-test; $*P \leq 0.05$, $**P \leq 0.01$, $***P \leq 0.001$, n.s. not significant. Mean ± s.d

the liver or adipose tissues of the HFHFD group compared to those of the control (Fig. S4C–G). No significant differences in glycogen accumulation in the liver or food and fructose water intake were observed between *Mkrn1* KD and control mice (Fig. S4H-N). Notably, histochemical and qRT-PCR analyses confirmed that *Mkrn1* KD in the liver suppressed steatosis, fibrosis, and inflammation compared to controls in mice fed a HFHFD (Fig. 3D–K). Accordingly, serum AST, ALT, TG, and cholesterol levels were decreased in *Mkrn1* KD mice (Fig. 3L, M). Finally, an increase in AMPK stabilization and activation were detected in the liver of *Mkrn1*-depleted mice (Figs. 3N and S4O). Overall, these observations indicate that the liver-specific depletion of *Mkrn1* suppressed MASH induced by HFHFD.

Ebastine suppresses lipid accumulation by targeting the MKRN1 C-terminal domain

As liver-specific *Mkrn1* KD using AAV8 suppressed diet-induced MASH, MKRN1 was demonstrated to be a potential therapeutic target. Although AAV vectors are promising gene delivery tools for treating multiple diseases, clinical trials have exposed several limitations of AAV gene transfer, including immune-mediated toxicities [43–46]. Recently, drug repurposing research on antihistamines for various diseases has been ongoing, with several antihistamine drugs confirmed for safety and efficacy through clinical trials [35–37]. Therefore, we aimed to identify antihistamines that are effective in regulating lipid accumulation in HepG2 cells. Among them, ebastine effectively inhibited lipid accumulation (Fig. S5A, B) in a manner similar to *Mkrn1* KD (Fig. 4A, B). Notably, ebastine binds to MKRN1 with a binding energy of −5.40 kcal/mol, near the active site of the protein containing two specific hydrogen bonds (H-bonds) with arginine 298 (R298) and one H-bond with lysine 360 (K360), as revealed by molecular docking analysis (Figs. 4C, D and S6A). To determine whether the R298 and K360 sites of MKRN1 are critical for the regulation of lipid accumulation by ebastine, we reconstituted HepG2 cells with a mutant MKRN1 (MKRN1 AA) containing double mutations (R298A-K360A). In cells expressing MKRN1 WT, ebastine treatment reduced the increased lipid accumulation, whereas, in cells expressing MKRN1 AA, ebastine failed to reduce lipid accumulation (Fig. 4E, F). Based on these observations, we employed an Octet R8 Bio-layer interferometry (BLI) system to evaluate the binding affinity between the MKRN1 C-terminal fragment and ebastine, using the MKRN1 N-terminal fragment as a control. The binding data analysis revealed that ebastine was able to bind to the C-terminus with a KD of 7.6 μM but not interact with the N-terminus of MKRN1 (Fig. 4G). These results are consistent with the finding that the site where ebastine docks with MKRN1 is located in the C-terminus. Overall, these findings suggest that ebastine effectively inhibits lipid accumulation by targeting the C-terminus of MKRN1, making it a promising candidate for therapeutic intervention in MASH.

Ebastine induces destabilization of MKRN1 and activates AMPK

To investigate the regulatory relationship between ebastine and MKRN1 at the molecular level, HepG2 cells were treated with ebastine, and MKRN1 protein levels were examined. Treatment with ebastine decreased MKRN1 protein levels, which was reversed by the proteasome inhibitor MG132, indicating that ebastine induces destabilization in a proteasome-dependent manner without affecting MKRN1 mRNA levels (Fig. 5A–C). To elucidate the mechanism underlying ebastine-induced MKRN1 degradation, we assessed MKRN1 self-ubiquitination in the presence of ebastine. Ubiquitination analysis revealed that ebastine promoted the self-ubiquitination of MKRN1, whereas the MKRN1 E3 ligase-defective mutant (H307E) was unaffected (Fig. 5D, E). Moreover, using deletion mutants of MKRN1, we observed that ebastine induced the degradation of the MKRN1 C-terminal fragment (264–482), which contains a RING domain with E3 ligase activity (Fig. 5F, G), and directly induced self-ubiquitination of the MKRN1 C-terminus (Fig. 5H). In addition, the MKRN1 AA mutant did not undergo further ubiquitination or degradation by ebastine, corroborating the results of the molecular docking analysis. (Figs. 4C–F and 5I, J).

The dissolution of lipid droplets was impeded by the use of an AMPK inhibitor (compound C), regardless of the presence of ebastine or absence of MKRN1, indicating that AMPK is a major factor influencing the reduction in lipid droplets (Fig. 6A, B). Both ebastine administration and MKRN1 suppression in HepG2 cells led to the stabilization and activation of AMPKα, without any detectable impact on its mRNA levels (Figs. 6C and S7A–C). Furthermore, when 293T cells expressing MKRN1 WT were treated with

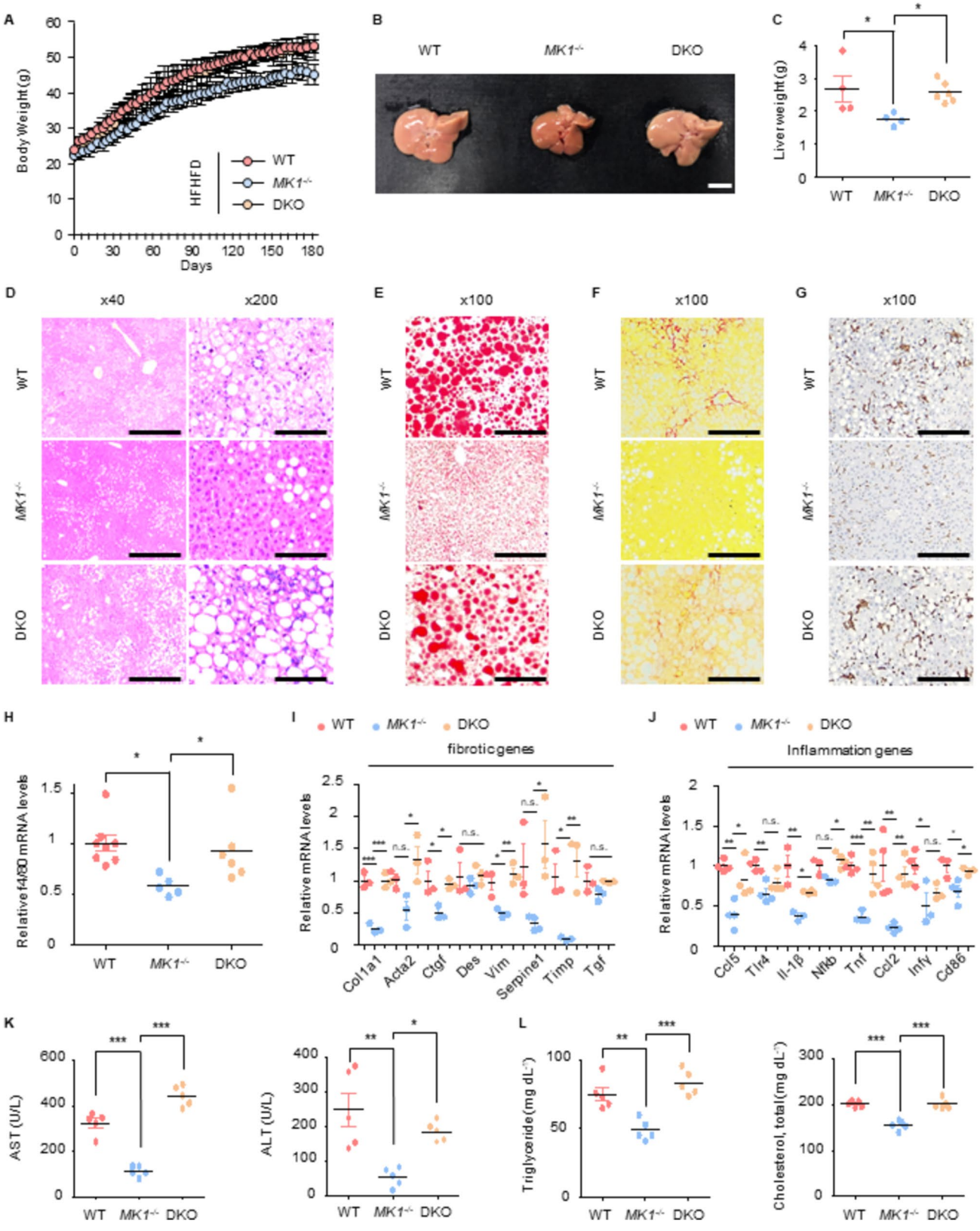
A
Body Weight (g)
Days
HFHFD
WT
MK1-/-
DKO
B
WT
MK1-/-
DKO
C
Liver weight (g)
D
x40
x200
E
x100
F
x100
G
x100
H
Relative f4/80 mRNA levels
I
fibrotic genes
Relative mRNA levels
Col1a1
Acta2
Ctgf
Des
Vim
Serpine1
Timp
Tgf
J
Inflammation genes
Ccl5
Tlr4
Il-1β
Nfkb
Tnf
Ccl2
Infγ
Cd86
K
AST (U/L)
ALT (U/L)
L
Triglyceride (mg dL-1)
Cholesterol, total (mg dL-1)

◂**Fig. 2** Prevention of MASH in *MK1*$^{-/-}$ mice was abrogated in *Mkrn1-Ampkα2* DKO mice. **A** The body weights of mice administered the HFHFD were measured every four days (n = 3–4 mice per group). **B** Representative images of the livers of WT, *MK1*$^{-/-}$, and DKO mice (Scale bar = 1 cm). **C** Liver weights. (n = 4–6 mice per group). **D** Representative images of H&E staining of the livers. (Scale bars; × 40 = 250 μm and × 200 = 25 μm). **E** Representative images of Oil Red O staining of the livers (Scale bars = 100 μm). **F** Representative images of Sirius red staining of the livers (Scale bar = 100 μm). **G** Representative images of f4/80 staining of the livers (Scale bar = 100 μm). **H** mRNA expression levels of f4/80 in the livers (n = 5–8 mice per group). **I** mRNA expression levels for fibrosis-related markers (n = 3–4 mice per group). **J** mRNA expression levels for inflammation-related markers (n = 3–4 mice per group). **K** AST and ALT serum levels (n = 5 mice per group). **L** Plasma concentrations of TG and cholesterol (n = 5 mice per group). One-way ANOVA with Dunnett's multiple comparison test; *$P \le 0.05$, **$P \le 0.01$, ***$P \le 0.001$, n.s. not significant

ebastine, AMPKα2 levels increased, accompanied by a decrease in MKRN1 WT expression. However, no changes in the levels of MKRN1 AA mutant and AMPKα2 were noted (Fig. S7D).

We further evaluated the effect of ebastine on the association between MKRN1 and AMPKα expression. Ebastine prevented the MKRN1-mediated degradation of AMPKα2 (Fig. 6D) as well as the MKRN1-mediated and endogenous ubiquitination of AMPKα2 (Fig. 6E, F). To determine whether ebastine could also inhibit MKRN1 function in mouse cells, WT or *MK1*$^{-/-}$ mouse embryonic fibroblasts (MEFs) were generated, and lipid droplet accumulation was measured. *MK1*$^{-/-}$ MEFs displayed decreased levels of lipid droplets compared to the WT MEFs. While ebastine was able to decrease lipid droplets in WT MEFs, it exhibited no effect on lipid accumulation in the *MK1*$^{-/-}$ MEFs (Fig. 6G, H). When WT MEFs were treated with ebastine, AMPKα2 levels were increased, but there was no effect in *MK1*$^{-/-}$ MEFs (Fig. 6I). Overall, ebastine promoted the degradation of MKRN1, resulting in the stabilization and activation of AMPKα and a subsequent reduction in lipid accumulation.

Ebastine treatment protects against HFHFD-induced MASH

As the results indicated that ebastine could prevent lipid accumulation in mouse cells, possibly by suppressing MKRN1, we subsequently tested its effects in mice. Mice were fed a HFHFD for 16 weeks followed by 4 additional weeks of HFHFD accompanied by daily intraperitoneal injections of ebastine at concentrations of 1 and 5 mg/kg (Fig. 7A). Mice fed a HFHFD for 16 weeks exhibited steatosis with fibrosis (Fig. 7A). However, there were no noticeable changes in body weight between the ebastine injection and control groups, with both groups maintaining a consistent average food and fructose water consumption (Figs. 7B and S8A, B). Notably, the livers of mice subjected to ebastine injection were smaller in size compared to those of the control group (Fig. 7C, D). Furthermore, this reduction in liver size coincided with a decrease in MKRN1 levels and an increase in the accumulation of AMPKα in the liver (Figs. 7E, F and S8C). Histochemistry and qRT-PCR results indicated that the mouse livers injected with ebastine were protected against steatosis, fibrosis, and inflammation (Fig. 7G–M). Accordingly, serum AST, ALT, TG, and cholesterol levels were decreased in mice injected with ebastine (Fig. S8D, E). Overall, these results suggest that ebastine binds to the C-terminus of MKRN1, specifically at the R298 and K360 sites, promoting self-ubiquitination followed by MKRN1 degradation, and leading to the stabilization of AMPKα. Furthermore, ebastine protected the mouse liver from the HFHFD-induced MASH, indicating a possible therapeutic application of this drug for MASH treatment.

We further investigated the effect of ebastine in MASH using a choline-deficient, L-amino acid-defined, HFD (CDAHFD) for 6 weeks. Initially, when WT or *MK1*−/− mice were fed CDAHFD, they maintained normal body and liver weights (Fig. S9A-C). However, *MK1*−/− mice were protected against steatosis in the liver phenotype and had lower serum AST, ALT, TG, and cholesterol levels than those in WT mice (Fig. S9D-G). pAMPKα levels were also increased in the livers of *MK1*−/− mice (Fig. S9H). MASH signatures were consequently analyzed in CDAHFD-fed mice, revealing pronounced fibrosis and inflammation in WT mice than in *MK1*−/− mice, as detected by Sirius red, f4/80, and qRT-PCR analyses (Fig. 9SI–M). To determine whether ebastine could inhibit MASH induced by CDAHFD, we subjected WT and *AMPKα2*−/− mice to intraperitoneal injections of ebastine at a concentration of 1 mg/kg for 2 weeks (Fig. S9N). Both WT and *AMPKα2*−/− mice maintained normal body and liver weights regardless of ebastine injection (Fig. S9O-Q). However, histological and mRNA analyses revealed that ebastine injections alleviated steatosis, fibrosis, and inflammation in the livers of WT mice, which are characteristic features of MASH (Fig. S9R, S). Moreover, ebastine injections increased AMPK activity in the livers of WT mice; however, these effects were absent in *AMPKα2*−/− mice (Fig. S9T). In summary, depletion of *Mkrn1* or administration of ebastine effectively protected the liver from HFHFD- and CDAHFD-induced MASH by promoting AMPK activity.

Discussion

AMPK is a key regulator of systemic and cellular energy homeostasis. As AMPK enhances catabolic processes by suppressing the production of macromolecules, it has been identified as an attractive therapeutic target for the treatment

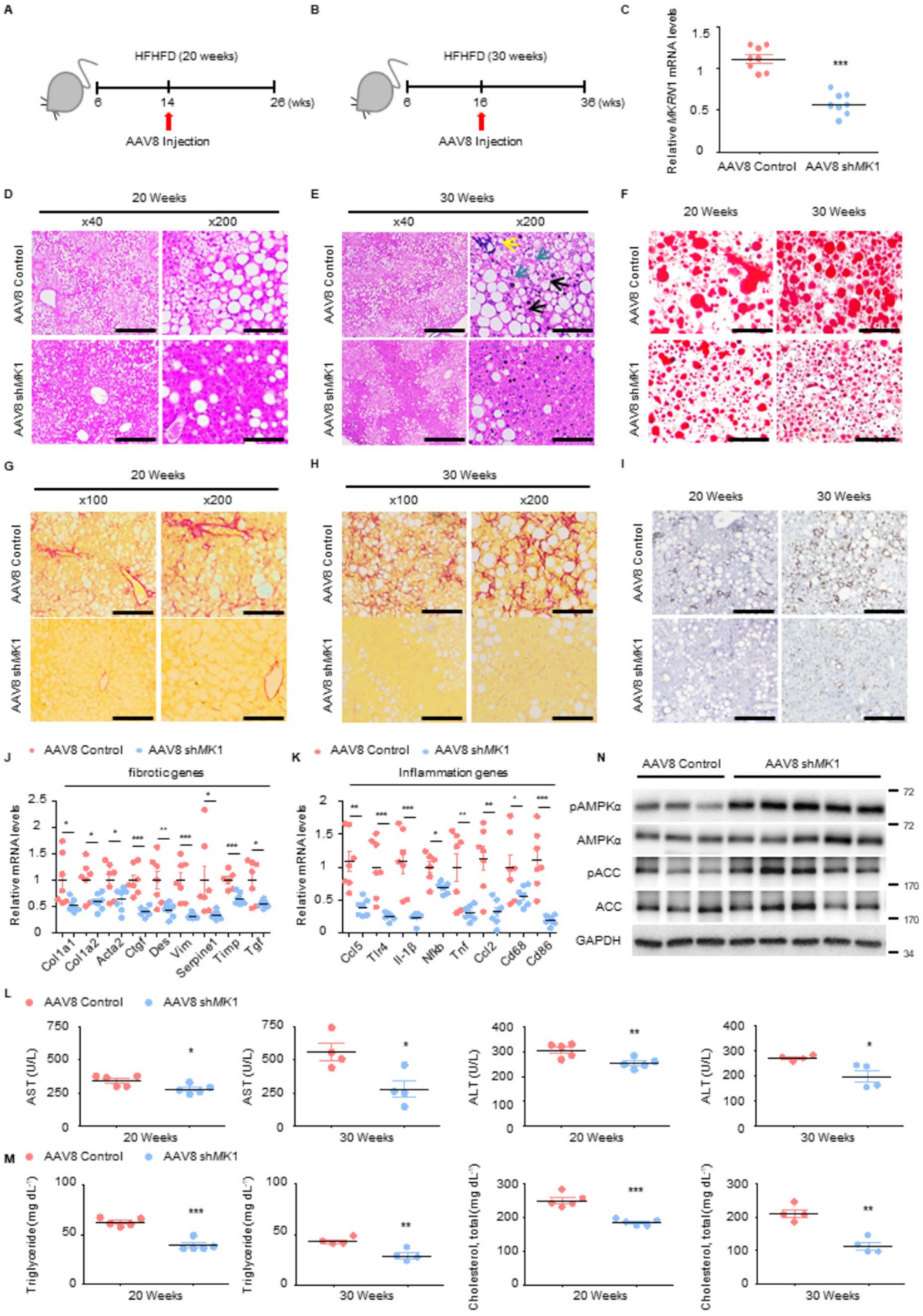
A
HFHFD (20 weeks)
6
14
26 (wks)
AAV8 Injection
B
HFHFD (30 weeks)
6
16
36 (wks)
AAV8 Injection
C
Relative MKRN1 mRNA levels
AAV8 Control
AAV8 shMK1
D
20 Weeks
x40
x200
AAV8 Control
AAV8 shMK1
E
30 Weeks
x40
x200
F
20 Weeks
30 Weeks
G
20 Weeks
x100
x200
H
30 Weeks
x100
x200
I
20 Weeks
30 Weeks
J
AAV8 Control
AAV8 shMK1
fibrotic genes
Relative mRNA levels
Col1a1
Col1a2
Acta2
Ctgf
Des
Vim
Serpine1
Timp
Tgf
K
Inflammation genes
Ccl5
Tlr4
Il-1β
Nfkb
Tnf
Ccl2
Cd68
Cd86
N
pAMPKα
AMPKα
pACC
ACC
GAPDH
L
AST (U/L)
ALT (U/L)
20 Weeks
30 Weeks
M
Triglyceride(mg dL⁻¹)
Cholesterol, total(mg dL⁻¹)

◂**Fig. 3** Ablation of hepatic *Mkrn1* improves hepatic steatosis, fibrosis, and inflammation in mice with diet-induced MASH. **A B** Schematic illustration of the experiment in which mice were fed HFHFD for 20 (**A**) or 30 (**B**) weeks and injected with AAV8 (AAV8 control or AAV8 sh*MK1*) at week 8 (**A**) or 10 (**B**). **C** mRNA expression levels of MKRN1 in the livers (n = 8 mice per group). **D**, **E** Representative images of H&E staining of the livers of mice fed the HFHFD for 20 (**D**) or 30 (**E**) weeks (Scale bars; × 40 = 250 μm and × 200 = 25 μm). **F** Representative images of Oil Red O staining of the livers of mice fed the HFHFD for 20 (left) or 30 (right) weeks (Scale bars = 100 μm). **G H** Representative images of Sirius red staining of the livers of mice fed the HFHFD for 20 (**G**) or 30 (**H**) weeks (Scale bars; × 100 = 100 μm; and × 200 = 25 μm). **I** Representative images of f4/80 staining of the livers of mice fed the HFHFD for 20 (left) or 30 (right) weeks. (Scale bar = 100 μm). **J** mRNA expression levels for fibrosis-related markers (n = 7 mice per group). **K** mRNA expression levels for inflammation-related markers (n = 7 mice per group). **L** AST and ALT serum levels (n = 4 mice per group). **M** Plasma concentrations of TG and cholesterol (n = 4 mice per group). **N** Lysates of the liver tissues analyzed by western blotting. Two-tailed Student's *t*-test; $*P \leq 0.05$, $**P \leq 0.01$, $***P \leq 0.001$, n.s. not significant. Mean ± s.d

of MASH [13]. AMPK activation regulates liver lipid metabolism by promoting fatty acid oxidation, inhibiting fatty acid synthesis, and reducing hepatic fat accumulation. It also improves insulin sensitivity and the underlying metabolic dysfunctions associated with MASLD. Furthermore, AMPK activation suppresses hepatic inflammation, mitigates liver damage, and slows MASLD progression [13, 30, 47]. It also inhibits the activation of hepatic stellate cells upon liver cell damage, reduces hepatic collagen production, prevents fibrosis, and ultimately preserves liver function [12, 48]. Studies using *Ampkα2* KO mice have provided further evidence of the correlation between AMPK deficiency and MASLD. AMPK deletion in mice leads to features resembling those of MASLD, including hepatic steatosis, inflammation, oxidative stress, and insulin resistance. Mechanistically, AMPK deficiency impairs fatty acid oxidation, disrupts glucose metabolism, and promotes inflammation, all of which contribute to MASLD development [42]. Therefore, targeting AMPK for therapeutic interventions may potentially treat MASH by restoring AMPK activity and alleviating the underlying metabolic abnormalities.

However, targeting AMPK for MASH treatment is challenging owing to the pleiotropic nature of AMPK signaling, limited tissue specificity, and complex regulation, in addition to the heterogeneous nature of the disease [18]. Direct modulation of AMPK expression may lead to unintended side and off-target effects in other organs [49, 50]. The dysregulation of AMPK in MASH is complex and requires a comprehensive approach that considers the upstream and downstream signaling components. Furthermore, MKRN1 depletion reduces hepatic mRNA levels of pro-inflammatory cytokines, indicating a potential indirect anti-inflammatory effect mediated by AMPK modulation. The alleviation of MASH symptoms in hepatocytes due to MKRN1 depletion may suppress cell death and subsequent immune responses, as reflected in the decreased f4/80 expression observed in our analyses. Although MKRN1 depletion may also directly affect Kupffer cell activation, additional studies using cell type-specific knockout models are required to clarify the role of MKRN1 in hepatic inflammation.

Despite the difficulties in modulating AMPK for clinical applications, targeting factors that regulate PTMs of AMPK might offer clinically favorable opportunities. First, PTMs play a crucial role in the regulation of AMPK activity and function, making them attractive therapeutic targets. The modulation of PTMs enables the fine-tuning of AMPK activity in a more precise manner, thereby minimizing off-target effects. Second, the PTM regulatory mechanisms may allow for the modulation of AMPK in a more context-dependent manner, enabling tailored therapeutic interventions for different diseases. For example, deubiquitinases, such as USP10 and USP7, remove ubiquitin from AMPK to stabilize and preserve its activity [33, 51]. The acetylation of AMPK is governed by acetyltransferases such as the p300/CBP-associated factor (PCAF) and SIRT1 [52]. These regulatory enzymes and their modifications play crucial roles in modulating AMPK activity, stability, and function under various physiological and pathological conditions. Finally, because PTMs have a reversible action, targeting PTM-regulating factors has the advantage of dynamic control and potential reversibility of AMPK signaling, enhancing the flexibility and adaptability of therapeutic approaches.

Developing new drugs presents significant challenges, including high costs, prolonged development timelines, and a high failure rate in clinical trials. Consequently, drug repurposing offers notable advantages, such as reduced development time and cost, as it involves identifying new therapeutic uses for existing drugs with known safety profiles. This approach accelerates the availability of treatments and mitigates the risks associated with de novo drug development [53]. Recent research has explored the repurposing of antihistamines for various therapeutic applications beyond their original use [37]. For instance, some antihistamines can be repurposed for Parkinson's disease, leveraging their ability to decrease oxidative stress and inflammation [54]. Additionally, antihistamines such as loratadine have been investigated for their potential in cancer treatment, demonstrating their ability to modulate immune responses [35, 55]. Ebastine has also been repurposed for various conditions, including cancers [35, 38, 39]. For example, it has shown promise in reducing inflammation and modulating immune responses in diseases beyond its original use for allergies [56]. Despite these advancements, there has been no prior research on the role of ebastine in regulating MASH. Our study revealed that ebastine binds to MKRN1, promoting its destabilization and subsequent degradation by stimulating its ubiquitination. This process enhances the stability

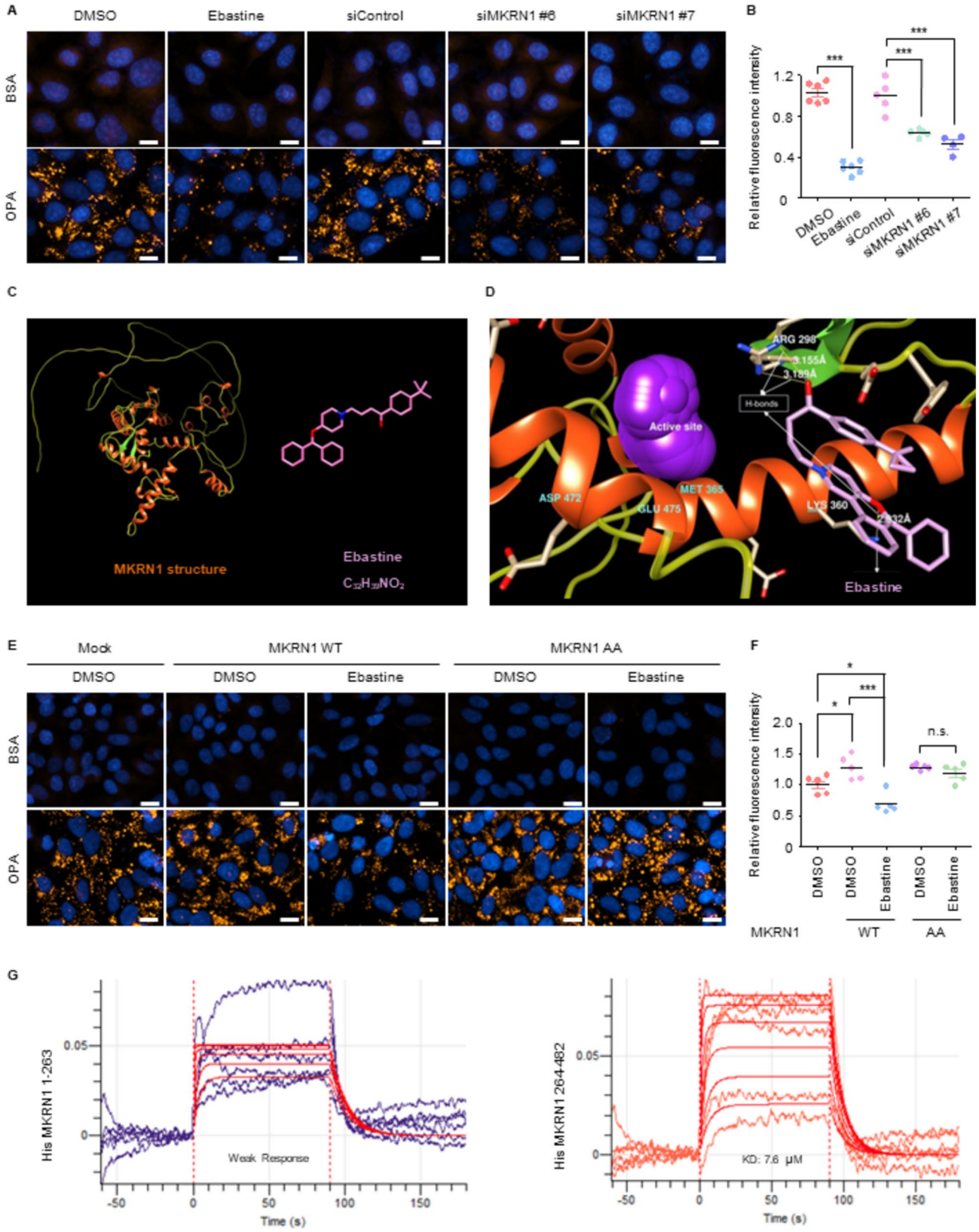
A
DMSO
Ebastine
siControl
siMKRN1 #6
siMKRN1 #7
BSA
OPA
B
Relative fluorescence intensity
1.2
0.8
0.4
0
***
***
***
DMSO
Ebastine
siControl
siMKRN1 #6
siMKRN1 #7
C
MKRN1 structure
Ebastine
$C_{32}H_{39}NO_2$
D
ARG 298
3.155Å
3.189Å
H-bonds
Active site
ASP 472
GLU 475
MET 365
LYS 360
2.932Å
Ebastine
E
Mock
MKRN1 WT
MKRN1 AA
DMSO
DMSO
Ebastine
DMSO
Ebastine
BSA
OPA
F
Relative fluorescence intensity
2.0
1.5
1.0
0.5
0
*
***
*
n.s.
DMSO
DMSO
Ebastine
DMSO
Ebastine
MKRN1
WT
AA
G
His MKRN1 1-263
0.05
0
Weak Response
-50
0
50
100
150
Time (s)
His MKRN1 264-482
0.05
0
KD: 7.6 μM
-50
0
50
100
150
Time (s)

◂**Fig. 4** Ebastine suppresses lipid accumulation by targeting the MKRN1 C-terminal domain. **A** Representative fluorescence microscopy images of HepG2 cells treated with ebastine or siMKRN1 (Scale bar = 10 μm). **B** Quantitative analysis of the relative fluorescence intensity of OPA-treated cells in **A**. **C** Alpha-fold protein structure of protein MKRN1 (left) retrieved from AlphaFold Protein Structure Database, and 3-dimensional structure of ebastine (right) retrieved from DrugBank database. **D** Visual representation of MKRN1 protein after docking with ebastine. Molecular docking analysis was conducted using Autodock 1.5.7 and Chimera 1.17.3. **E** Representative fluorescence microscopy images of HepG2 cells transfected with plasmids expressing HA/MKRN1 WT or HA/MKRN1 AA mutant with or without ebastine. (Scale bar = 10 μm). **F** Quantitative analysis of the relative fluorescence intensity of OPA-treated cells in **E**. **G** BLI analysis using recombinant His/MKRN1 1–263 or His/MKRN1 264–482 with ebastine. At least three independent experiments were performed, with a minimum of 300 cells analyzed per group for quantitative analysis. One-way ANOVA with Dunnett's multiple comparison test; $*P \le 0.05$, $**P \le 0.01$, $***P \le 0.0001$, n.s. not significant

and activity of AMPK, which subsequently suppresses lipid accumulation, inflammation, and fibrosis. These findings suggest that ebastine could be a promising therapeutic agent for the treatment of MASH.

Materials and methods

Experimental animals

Mkrn1 whole body KO mice were obtained from T. A. Gray (David Axelrod Institute, USA) [57]. *Mkrn1* homozygous KO mice ($MK1^{-/-}$) and their WT littermates ($MK1^{+/+}$) were produced by mating *Mkrn1* heterozygous KO mice ($MK1^{\pm}$). The following forward primers were used for the genotype analysis of the *Mkrn1* gene: 5′-TGACAGGCCACAGTG AACTC-3′, 5′-GGCAAAGCTGCTTCTTTGTCTCC-3′, and 5′-CAAAGGGAAAGGGTAAAGTGGTAGGG-3′. These primers amplified DNA fragments of approximately 1000 and 820 base pairs in $MK1^{-/-}$ and $MK1^{+/+}$ mice, respectively. *Ampkα2* KO mice were obtained from Benoit Viollet (INSERM, Paris, France) [17]. *Ampkα2* and *Mkrn1* DKO mice were generated by crossing *Ampkα2* and *Mkrn1* heterozygous mice. The following forward primers were used for the genotype analysis of the *Ampkα2* gene: 5′-GCTTAGCAC GTTACCCTGGATGG-3′, 5′-GTTATCAGCCCAACTAAT TACAC-3′, and 5′-GCATTGAACCACAGTCCTTCCTC-3′. To induce MASH in mice, they were subjected to a HFD and 30% to high fructose water (HFHFD) for 20 or 30 weeks or a choline-deficient, L-amino acid-defined, HFD (CDAHFD; Research DIET Inc., NJ, USA) for 6 weeks. In the context of adeno-associated virus 8 (AAV8) experiments, six-week-old male C57BL/6 mice were confined in individual enclosures. The shRNA sequences were as follows: AAV8 Control: 5′- GCAAGCTGACCCTGAAGTTCATTCAAG AGATGAACTTCAGGGTCAGCTTGCTTTTT-3′ and AAV8 sh*MK1*: 5′-GCGAGATGTTGCTTATGCTTTCTC GAGAAAGCATAAGCAACATCTCGCTTTTT-3′. These mice were fed a HFHFD for either 8 or 10 weeks. AAV8 was then administered to the mice via injection into the tail vein. Following 12 or 20 weeks of continuous consumption of the HFHFD, mice were euthanized for further studies. We randomly assigned mice to the experimental groups and the MASLD studies were blinded. The mice were housed in environments with controlled temperature and illumination (standard 12-h light-12 h dark cycles). They were provided ad libitum access to both sustenance and water.

Cell culture

$MK1^{\pm}$ mice were bred to generate mouse embryonic fibroblasts (MEFs) with or without MKRN1 expression. To obtain MEFs on day 13.5 from the embryos, embryos were minced after being rinsed with phosphate-buffered saline (PBS; Welgene) and incubated with 3 ml trypsin/EDTA (Gibco) at 37 °C for 15 min. MEFs were grown in 20 ml Dulbecco's modified Eagle medium (DMEM; GIBCO) containing 10% fetal bovine serum (FBS; GIBCO) for 4–8 h before the medium was replaced with DMEM containing 10% FBS. The confluent MEFs were subsequently subcultured at a ratio of 1:3. 293T (a cell line derived from human embryonic kidneys) and HepG2 (a cell line derived from human hepatocellular carcinoma) cells were obtained from the American Type Culture Collection (ATCC, Manassas, VA). The phenotypes of these cell lines were authenticated by ATCC on a regular basis. All cell lines used in this study were negative for mycoplasma when detected using an e-Myco plus Mycoplasma PCR Detection Kit (Intron, Gyeonggi-do, Republic of Korea) and were protected from mycoplasma infection by treatment with PlasmocinTM (InvivoGen, CA, USA). To transfect plasmid DNA or short interfering (si)RNA, either PEI (Sigma-Aldrich, St. Louis, MO, USA) or Lipofectamine RNAiMAX (Invitrogen) was utilized.

Reagents

Phospho-AMPKα (2535), AMPKα (2603), AMPKα2 (2757), phospho-ACC (3661), ACC (3676), f4/80 (70076), HRP-conjugated-ubiquitin (3738) antibodies were purchased from Cell Signaling Technology (Danvers, MA, United States). Sigma-Aldrich supplied the FLAG (F3165 and F7425), β-actin (A5316) antibodies and ebastine (Y0002031). The MKRN1 antibodies (A300-990A, NBP2-45816) were procured from Bethyl Laboratories, NOVUS biologicals, and Abcam, respectively. The HRP-conjugated-HA antibody (12,013,819,001) was obtained from Roche. Antibodies against GAPDH (sc-25778), GFP (sc-8334), and

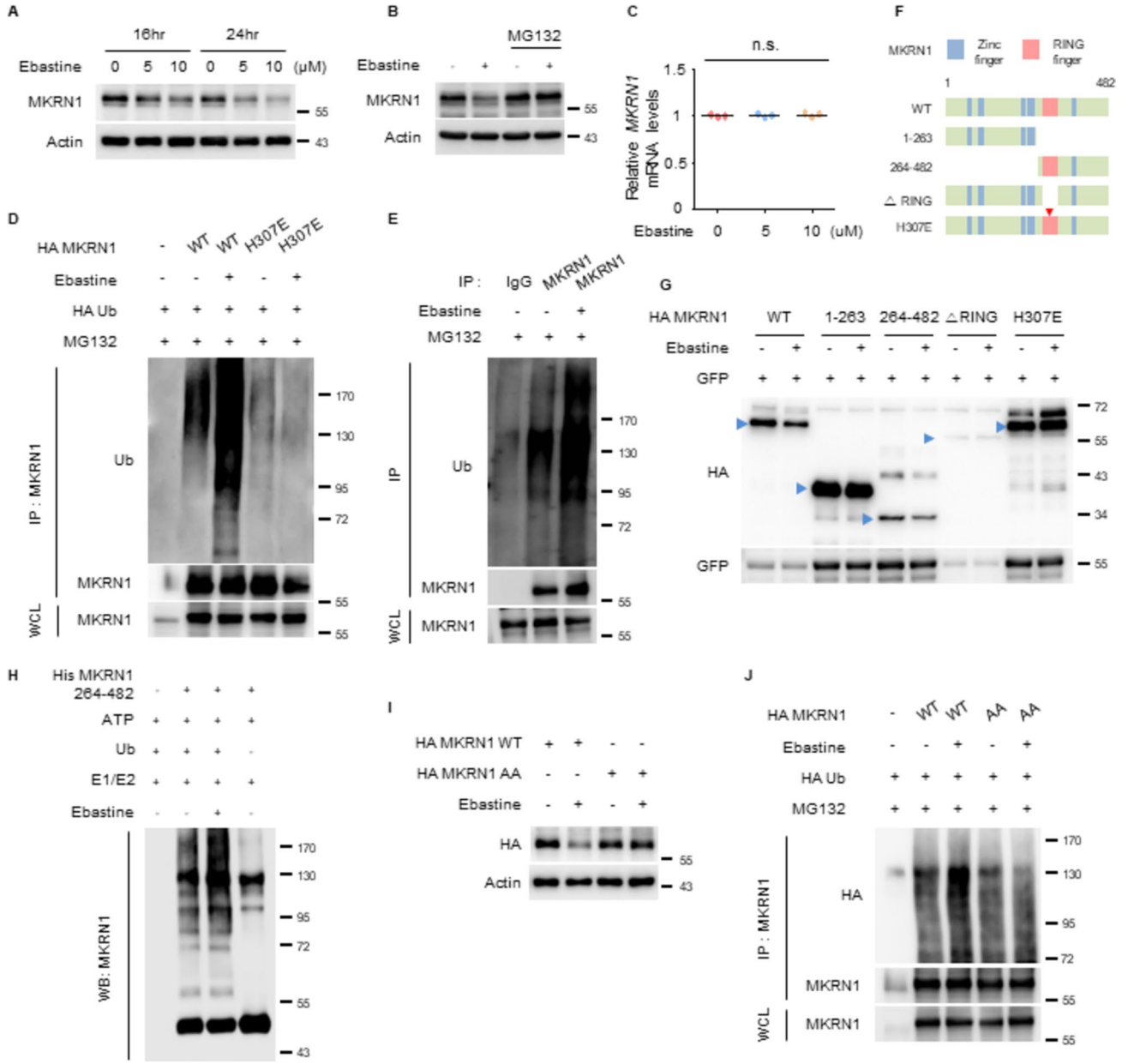

Fig. 5 Ebastine induces MKRN1 destabilization. **A** HepG2 cells were treated with 0, 5, or 10 μM ebastine for 16 h or 24 h followed by western blotting. **B** HepG2 cells were treated with 10 μM ebastine for 24 h in the presence or absence of 20 μM MG132 for 6h followed by western blotting. **C** The MKRN1 mRNA levels were analyzed via qRT-PCR in the presence or absence of ebastine in HepG2 cells (n = 3 per group). **D** 293T cells were transfected with plasmids expressing HA/MKRN1 WT, HA/MKRN1 H307E mutant, and HA/Ub with or without ebastine. After 18 h, the transfected cells were treated with MG132 for 6h in the presence or absence of ebastine. Cell lysates were immunoprecipitated using anti-MKRN1 antibodies followed by western blotting using anti-Ub antibodies. **E** Ubiquitinated endogenous MKRN1 was determined under denaturing conditions using MG132-treated HepG2 cells. Immunoprecipitation of cell lysates with anti-MKRN1 antibodies was followed by western blotting with anti-Ub antibodies. **F** Schematic illustrations of MKRN1 WT and its mutants. **G** 293T cells were transfected with plasmids expressing HA/MKRN1 WT and its mutants followed by ebastine treatment. **H** In vitro ubiquitination analysis of recombinant MKRN1 C-terminus (264–482) in the presence or absence of E1, E2, Ub, ATP, or ebastine. **I** 293T cells were transfected with plasmids expressing HA/MKRN1 WT or HA/MKRN1 AA mutant followed by ebastine treatment. **J** 293T cells were transfected with plasmids expressing HA/MKRN1 WT, HA/MKRN1 AA mutant, and HA/Ub with or without ebastine. After 18 h, the transfected cells were treated with MG132 for 6h in the presence or absence of ebastine. Cell lysates were immunoprecipitated using anti-MKRN1 antibodies followed by western blotting using anti-HA antibodies. One-way ANOVA with Dunnett's multiple comparison test; n.s. not significant

HA (sc-805) were purchased from Santa Cruz Biotechnology (Dallas, TX, USA). MG132 (M-1157) was purchased from A.G. Scientific (CA, United States).

Plasmid constructs

pcDNA3.1/MKRN1, pcDNA3-HA/MKRN1 WT, pcDNA3-HA/MKRN1 1–263, pcDNA3-HA/MKRN1 264–482, pcDNA3-HA/MKRN1 ΔRING, pcDNA3-HA/MKRN1 H307E, and pcDNA3-FLAG/AMPKα2 have been described previously [34]. pET32a-His/MKRN1 c-termimus (264–482) was subcloned from pcDNA3–HA/MKRN1. The pRK5-HA/Ub construct was provided by B. J. Hwang (Kangwon University, Korea). All siRNAs were obtained from Qiagen (Valencia, CA, USA), and the sequences were as follows: human MKRN1 #6, 5′-CGGGATCCTCTCCAACTGCAA-3′; #7, 5′-CACAGGCGAAGCTGAGTCAAG-3′.

Quantitative Real-Time PCR (qPCR) analysis

RNA was obtained from tissues and cells using the TRIzol reagent according to the manufacturer's instructions (Invitrogen, Carlsbad, CA, USA). cDNA was amplified using 1 μg of total RNA and analysed using the QuantiTect SYBR Green PCR Kit. Real-time PCR (Rotor-GeneQ 2plex, Qiagen) was performed with custom Primetime qPCR Primers (IDT, Coralville, IA, USA). The following primers: mouse Gapdh, 5′-AATGGTGAAGGTCGGTGTG-3′ and 5′-GTGGAGTCATACTGGAACATGTAG-3′; mouse *Mkrn1*, 5′-GTGAATGCCATTGAGTTTGTCC-3′ and 5′-CTCCTTCTCTGACTCTTCCTTG-3′; mouse *Ampkα2*, 5′-CCAACAACATCTAAACTGCGAA-3′ and 5′-GTGAAGATCGGACACTACGTG-3′; mouse *f4/80*, 5′-ATTCACTGTCTGCTCAACCG-3′ and 5′-GGAAGTGGATGGCATAGATGA-3′; mouse *Col1a1*, 5′-CATTGTGTATGCAGCTGACTTG-3′ and 5′-CGCAAAGAGTCTACATGTCTAGG-3′; mouse *Col1a2*, 5′-AGTAACTTCGTGCCTAGCAAC-3′ and 5′-CATCAACACCATCTCTGCCT-3′; mouse *Acta2*, 5′-GAGCTACGAACTGCCTGAC-3′ and 5′-CTGTTATAGGTGGTTTCGTGGA-3′; mouse *Ctgf*, 5′-GTTACCAATGACAATACCTTCTGC-3′ and 5′-TTGACAGGCTTGGCGATT-3′; mouse *Des*, 5′-TCAACCTTCCTATCCAGACCT-3′ and 5′-GCTGACAACCTCTCCATCC-3′; mouse *Vim*, 5′-ATCAGCTCACCAACGACAAG-3′ and 5′-TCAACATCCTGTCTGAATGACTG-3′; mouse *Serpine1*, 5′-CTATGGTGAAACAGGTGGACT-3′ and 5′-CGTGTCAGCTCGTCTACAG-3′; mouse *Timp*, 5′-AGACAGCCTTCTGCAACT-3′ and 5′-CAGCCTTGAATCCTTTTAGCATC-3′; mouse *Tgf*, 5′-CCGAATGTCTGACGTATTGAAGA-3′ and 5′GCGGACTACTATGCTAAAGAGG-3′; mouse *Ccl5*, 5′-GCTCCAATCTTGCAGTCGT-3′ and 5′-CCTCTATCCTAGCTCATCTCCA-3′; mouse *Tlr4*, 5′-GAAGCTTGAATCCCTGCATAG-3′ and 5′-AGCTCAGATCTATGTTCTTGGTTG-3′; mouse *Il-1β*, 5′-GACCTGTTCTTTGAAGTTGACG-3′ and 5′-CTCTTGTTGATGTGCTGCTG-3′; mouse *Nfκb*, 5′-TGTCTGCCTCTCTCGTCTT-3′ and 5′-GAGTTTGCGGAAGGATGTCT-3′; mouse *Tnf*, 5′-TCTTTGAGATCCATGCCGTTG-3′ and 5′-AGACCCTCACACTCAGATCA-3′; mouse *Ccl2*, 5′-AACTACAGCTTCTTTGGGACA-3′ and 5′-CATCCACGTGTTGGCTCA-3′; mouse *Infγ*, 5′-CTGAGACAATGAACGCTACACA-3′ and 5′-TCCACATCTATGCCACTTGAG-3′; mouse *Cd68*, 5′-CACCTGTCTCTCTCATTTCCTT-3′, 5′-CCATGAATGTCCACTGTGCT-3′; mouse *Cd86*, 5′-CAGACTCCTGTAGACGTGTTC-3′, 5′-AACAGCATCTGAGATCAGCA-3′; human GAPDH, 5′-TGTAGTTGAGGTCAATGAAGGG-3′ and 5′-ACATCGCTCAGACACCATG-3′; human MKRN1, 5′- GAGCAGGTTCAGAGGACTGG-3′ and 5′- CACTCTCCCACTGCAGCATA-3′; human AMPKα2, 5′-CCAACAACATCTAAACTGCGAA-3′ and 5′-GTGAAGATCGGACACTACGTG-3′.

Histology and immunohistochemistry (IHC)

Tissues fixed in 10% buffered formalin were embedded in paraffin followed by staining with hematoxylin and eosin (H&E), Sirius red, F4/80, MKRN1, or periodic acid Schiff for glycogen detection. For Oil Red O staining, tissues were embedded in OCT compound and snapfrozen in liquid nitrogen. Frozen sections were stained with Oil Red O (SigmaAldrich).

Serum biochemistry

Fasting plasma triglyceride (TG) and total cholesterol (TC) concentrations were determined using enzymatic methods (Cobas c502 with ISE, Serial.no: 18J4-06, 18Y2-06) in overnight-fasted mice. Serum AST and ALT levels were measured using the absorbance method (Cobas c502 with ISE, Serial.no: 18J4-06, 18Y2-06) according to the recommended protocols from the International Federation of Clinical Chemistry.

Free fatty acid (FFA)-induced steatosis

For the FFA stock solution, oleic acid and palmitate (OPA, 100 mM) were conjugated with 1% (w/v) bovine serum albumin (BSA). The required volume of the FFA stock was added to the medium to obtain 1 mM concentration of fatty acids for experiments. HepG2 and MEF cells were treated with OPA complexed with BSA or fatty acid-free BSA (used as the control) for 24 h and then stained with 1mg/ml Nile Red (Sigma, 19123).

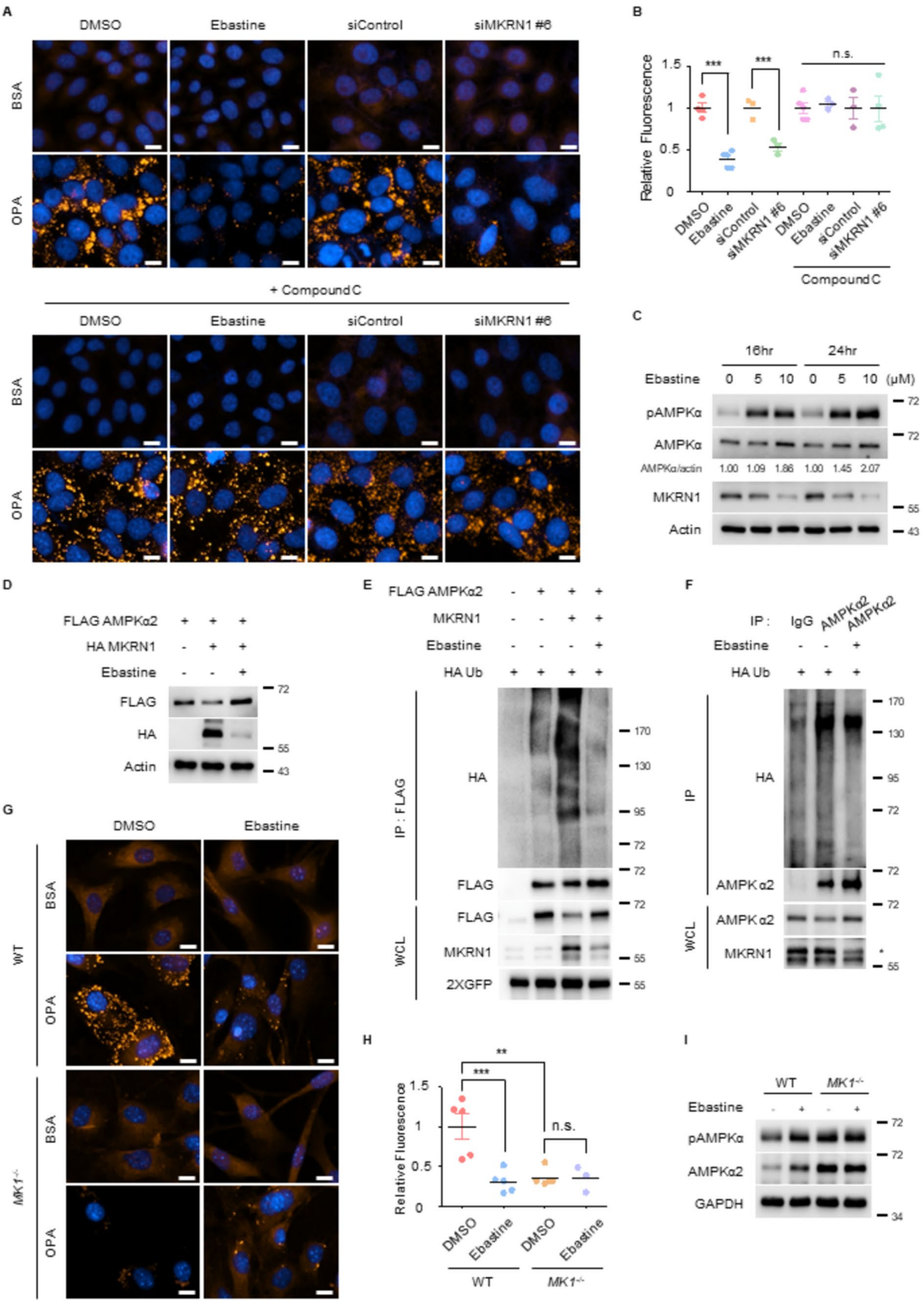
A
DMSO
Ebastine
siControl
siMKRN1 #6
BSA
OPA
+ Compound C
B
Relative Fluorescence
***
n.s.
Compound C
C
16hr
24hr
Ebastine
(μM)
pAMPKα
AMPKα
AMPKα/actin
MKRN1
Actin
D
FLAG AMPKα2
HA MKRN1
Ebastine
FLAG
HA
Actin
E
FLAG AMPKα2
MKRN1
Ebastine
HA Ub
IP : FLAG
WCL
HA
FLAG
MKRN1
2XGFP
F
IP :
IgG
AMPKα2
Ebastine
HA Ub
IP
WCL
HA
AMPK α2
MKRN1
G
WT
MK1-/-
H
Relative Fluorescence
**
***
n.s.
I
WT
MK1-/-
pAMPKα
AMPKα2
GAPDH

◂**Fig. 6** Ebastine prevents MKRN1-mediated ubiquitination and degradation of AMPKα2. **A**, **B** HepG2 cells treated with DMSO, ebastine, or siMKRN1 were incubated in the absence (top) or presence (bottom) of compound C with BSA or 1 mM OPA. Representative fluorescence microscopy images of HepG2 cells stained with Hoechst and Nile red (Scale bars = 10 μm) (**A**). Analysis of the relative fluorescence intensity of OPA-treated cells (**B**). **C** HepG2 cells were treated with 0, 5, or 10 μM ebastine for 16 h or 24 h followed by western blotting. **D** 293T cells were transfected with plasmids expressing FLAG/AMPKα2 and/or HA/MKRN1 with or without ebastine followed by western blotting. **E** 293T cells were transfected with plasmids expressing MKRN1 WT, FLAG/AMPKα2, and HA/Ub in the presence or absence of ebastine. Cell lysates were immunoprecipitated using anti-FLAG antibodies followed by western blotting using anti-HA antibodies. **F** HA/Ub-expressing plasmid was transfected into HepG2 cells in the presence or absence of ebastine. Immunoprecipitation of cell lysates with anti-AMPKα2 antibodies was followed by western blotting with anti-HA antibodies. **G**, **H** Representative fluorescence microscopy images of WT or *MK1*$^{-/-}$ MEFs stained with Hoechst and Nile red after treatment with BSA or 1 mM OPA and DMSO or ebastine (**G**), and quantitative analysis of the relative fluorescence intensity of OPA-treated cells (Scale bars = 10 μm) (**H**). **I** WT or *MK1*$^{-/-}$ MEFs were treated with ebastine followed by western blotting. At least three independent experiments were performed, with a minimum of 100 cells analyzed per group for quantitative analysis. One-way ANOVA with Dunnett's multiple comparison test; *$P \leq 0.05$, **$P \leq 0.01$, ***$P \leq 0.001$, n.s. not significant

Biolayered interferometry (BLI) analysis

The purified N-terminal- and C-terminal fragments of human MKRN1 were biotinylated using an EZ-Link™ Sulfo-NHS-LC-Biotinylation Kit (Thermo Fisher Scientific, USA, cat# 21435). Prior to the reaction with Biotin-PEG4-NHS, the buffer for the proteins was replaced with PBST buffer (PBS with 0.1% Tween 40) with 2% DMSO using a desalting column, PD-10 (Cytiva, USA). The Biotin-PEG4-NHS solution was mixed with 1 mg/ml of purified protein and incubated at room temperature for 1 h. The extra biotin molecules were removed using a desalting column (PD-10) in PBST buffer with 2% DMSO. The interactions between biotin-labeled MKRN1s and ebastine were monitored using BLI analysis performed with the Octet R8 system (Satorius, USA). Biotin-labeled proteins were immobilized on super streptavidin biosensors (Satorius, USA, cat #18–5057) with loading and dissociation performed for 600 and 300 s, respectively. The small-molecule association and dissociation processes were performed for 90 and 600 s, respectively. All binding sequences in 96-well were plated with 200 μl of total volume (Thermo Fisher Scientific, USA, cat #165305). The binding properties of small molecules were monitored at six concentrations (3.25, 7.5, 15, 30, 60, and 120 mM). The final concentration of DMSO for the binding measurements was set to 2%. The binding properties, such as the association rate constant (Kon), dissociation rate constant (Koff), and affinity constant (KD) were calculated by fitting the BLI seonsorigram to a 1:1 binding model. The goodness-of-fit was validated by monitoring the R2 value, which was higher than 0.95.

Ubiquitination assay

The ubiquitination assay was conducted under denaturing conditions to detect ubiquitinated endogenous and overexpressed proteins. Briefly, to detect proteins ubiquitinated with HA-conjugated ubiquitin or endogenously ubiquitinated proteins under denaturing conditions, cells were lysed by boiling for 10 min in PBS containing 1% SDS and 10 nM N-ethylmaleimide (NEM). The lysates were immunoprecipitated in lysis buffer (a final concentration of 0.1% SDS). For western blotting, proteins were transferred to polyvinylidene difluoride membranes and denatured using 6 M guanidine-HCl containing 20 mM Tris–HCl (pH 7.5), 5 mM β-mercaptoethanol, and 1 mM phenylmethyl sulphonyl fluoride for 30 min at 4 °C. Ubiquitinated proteins were identified using horseradish peroxidase-conjugated anti-Ub antibodies. For in vitro ubiquitination assays, a 0.5 μg sample of recombinant proteins purified using bacterial systems was incubated with 100 ng of E1 (UBE1, E-305, Boston Biochem, Cambridge, MA, USA), 250 ng of E2 (UbcH5c, E2-627, Boston Biochem), and 5 μg of ubiquitin (U-100H, Boston Biochem) in 20 μl of reaction buffer (40 mM of Tris, 50 mM of NaCl, 5 mM of $MgCl_2$, 2 mM of ATP and 1 mM of dithiothreitol, pH 7.6) as indicated. The reaction was stopped after 3 h at 37 °C by the addition of SDS sample buffer and boiling.

Protein purification and immunoprecipitation assay

His tagged recombinant MKRN1 C-terminal fragment (264–482) protein was purified from bacteria using Ni–NTA agarose.

For immunoprecipitation assay, the cells were lysed in lysis buffer (50 mM of TrisHCl [pH 7.5], 150 mM of NaCl, 0.5% Triton X-100, and 1 mM of EDTA) containing a protease inhibitor cocktail. The cell lysates were then incubated with 1 μg of antibody with rotation, followed by incubation with 25 μl of protein G agarose (Invitrogen), and the precipitated proteins were eluted in SDS sample buffer under conditions involving boiling.

Statistical analysis

Statistical analyses in this study were performed using either two-tailed tests or one-way ANOVA followed by Dunnett's multiple comparison test. Data are presented as means with 95% confidence intervals. All analyses were conducted using GraphPad Prism software (version 7.0; GraphPad Software

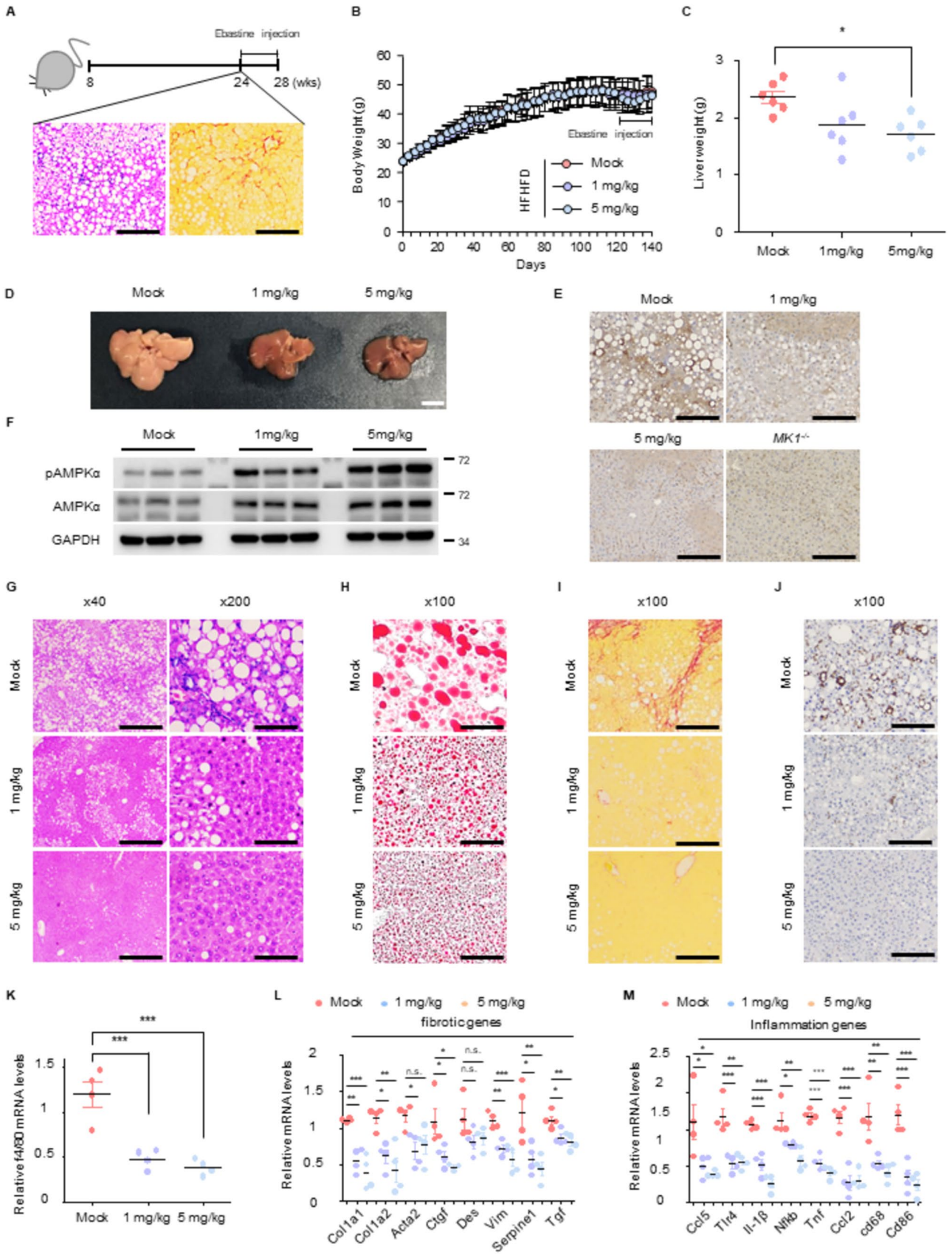
A
Ebastine injection
8
24
28 (wks)
B
Body Weight (g)
Ebastine injection
HFHFD
Mock
1 mg/kg
5 mg/kg
Days
C
Liver weight (g)
Mock
1mg/kg
5mg/kg
D
Mock
1 mg/kg
5 mg/kg
E
Mock
1 mg/kg
5 mg/kg
MK1-/-
F
Mock
1mg/kg
5mg/kg
pAMPKα
AMPKα
GAPDH
72
72
34
G
x40
x200
Mock
1 mg/kg
5 mg/kg
H
x100
I
x100
J
x100
K
Relative f4/80 mRNA levels
Mock
1 mg/kg
5 mg/kg
L
Mock
1 mg/kg
5 mg/kg
fibrotic genes
Relative mRNA levels
Col1a1
Col1a2
Acta2
Ctgf
Des
Vim
Serpine1
Tgf
M
Mock
1 mg/kg
5 mg/kg
Inflammation genes
Relative mRNA levels
Ccl5
Tlr4
Il-1β
Nfκb
Tnf
Ccl2
cd68
Cd86

◂**Fig. 7** Ebastine treatment protects against diet-induced MASH in vivo. **A** Schematic illustration of ebastine administration in mice fed a HFHFD. **B** The body weights of mice administered HFHFD were measured every four days (Mock, n = 8; ebastine 1mg/kg, n = 8; and ebastine 5mg/kg, n = 7). **C** Liver weights (n = 6 mice per group). **D** Representative image of the livers after treatment with mock or ebastine (Scale bar = 1 cm). **E** IHC staining for MKRN1 of the livers (Scale bar = 100 μm). **F** Lysates of liver tissues analyzed using western blotting. **G** Representative images of H&E staining of the livers (Scale bars; × 40 = 250 μm and × 200 = 25 μm). **H** Representative images of Oil Red O staining of the livers (Scale bars = 100 μm). **I** Representative images of Sirius red staining of the livers (Scale bars = 100 μm). **J** Representative images of f4/80 staining of the livers (Scale bar = 100 μm). **K** mRNA expression levels of f4/80 in the livers (n = 4 mice per group). **L** mRNA expression levels for fibrosis-related markers (n = 4 mice per group). **M** mRNA expression levels of inflammation-related markers (n = 4 mice per group). One-way ANOVA with Dunnett's multiple comparison test; $*P \leq 0.05$, $**P \leq 0.01$, $***P \leq 0.001$, n.s. not significant

Inc., La Jolla, CA). A *p*-value of less than 0.05 was considered statistically significant.

Supplementary Information The online version contains supplementary material available at https://doi.org/10.1007/s00018-024-05535-2.

Acknowledgements Not applicable.

Author Contributions Study concept and Design: SK, JS. Assisted with animal experiments: HH, HR, SBK. Molecular docking study: SM, SSL. Acquisition of BLI data: JK, DK. Critical review of the manuscript: JC, SSL, HK, SML.

Funding This work was supported by grants from the National Research Foundation of Korea (NRF) funded by: Ministry of Science, ICT, and Future Planning (MSIP) grant 2015R1A3A2066581. Korean government (MSIT) grant NRF-2020R1A5A1019023, RS-2024-00346972, and RS-2024-00509145. Brain Korea 21(BK21) FOUR program.

Availability of data and material All data required to evaluate the conclusions in the paper are present in the manuscript and the supplementary materials.

Declarations

Conflict of interests The authors declare no competing interests.

Ethical approval and consent to participate The Institutional Animal Care and Use Committees (IACUC) of the Laboratory Animal Research Center at Yonsei University conducted a comprehensive review and approved all procedures utilized in this study. (IACUC-A-201810-802-02).

Consent for publication Not applicable.

References

1. Zhang P et al (2021) Similarities and differences: a comparative review of the molecular mechanisms and effectors of NAFLD and AFLD. Front Physiol 12:710285. https://doi.org/10.3389/fphys.2021.710285
2. Rui L, Lin JD (2022) Reprogramming of hepatic metabolism and microenvironment in nonalcoholic steatohepatitis. Annu Rev Nutr 42:91–113. https://doi.org/10.1146/annurev-nutr-062220-105200
3. Perazzo H, Pacheco AG, Griep RH, Collaborators, (2023) Changing from NAFLD through MAFLD to MASLD: Similar prevalence and risk factors in a large Brazilian cohort. J Hepatol. https://doi.org/10.1016/j.jhep.2023.08.025
4. Loomba R, Friedman SL, Shulman GI (2021) Mechanisms and disease consequences of nonalcoholic fatty liver disease. Cell 184:2537–2564. https://doi.org/10.1016/j.cell.2021.04.015
5. Craciun A, Cortez-Pinto H (2022) Alarming increase of NASH as cause of liver cancer. Cell Rep Med 3:100723. https://doi.org/10.1016/j.xcrm.2022.100723
6. Schuppan D, Surabattula R, Wang XY (2018) Determinants of fibrosis progression and regression in NASH. J Hepatol 68:238–250. https://doi.org/10.1016/j.jhep.2017.11.012
7. Zhu C, Tabas I, Schwabe RF, Pajvani UB (2021) Maladaptive regeneration—the reawakening of developmental pathways in NASH and fibrosis. Nat Rev Gastroenterol Hepatol 18:131–142. https://doi.org/10.1038/s41575-020-00365-6
8. Le MH et al (2019) Global NAFLD prevalence: a systematic review and meta-analysis. Clin Gastroenterol Hepatol 20(2809–2817):e2828. https://doi.org/10.1016/j.cgh.2021.12.002
9. Younossi ZM et al (2023) The global epidemiology of nonalcoholic fatty liver disease (NAFLD) and nonalcoholic steatohepatitis (NASH): a systematic review. Hepatology 77:1335–1347. https://doi.org/10.1097/HEP.0000000000000004
10. Byrne CD, Targher G (2020) What's new in NAFLD pathogenesis, biomarkers and treatment? Nat Rev Gastroenterol Hepatol 17:70–71. https://doi.org/10.1038/s41575-019-0239-2
11. Vuppalanchi R, Noureddin M, Alkhouri N, Sanyal AJ (2021) Therapeutic pipeline in nonalcoholic steatohepatitis. Nat Rev Gastroenterol Hepatol 18:373–392. https://doi.org/10.1038/s41575-020-00408-y
12. O'Neill HM, Holloway GP, Steinberg GR (2013) AMPK regulation of fatty acid metabolism and mitochondrial biogenesis: implications for obesity. Mol Cell Endocrinol 366:135–151. https://doi.org/10.1016/j.mce.2012.06.019
13. Fang C et al (2022) The AMPK pathway in fatty liver disease. Front Physiol 13:970292. https://doi.org/10.3389/fphys.2022.970292
14. Herzig S, Shaw RJ (2018) AMPK: guardian of metabolism and mitochondrial homeostasis. Nat Rev Mol Cell Biol 19:121–135. https://doi.org/10.1038/nrm.2017.95
15. Foretz M, Viollet B (2011) Regulation of hepatic metabolism by AMPK. J Hepatol 54:827–829. https://doi.org/10.1016/j.jhep.2010.09.014
16. Steinberg GR, Hardie DG (2023) New insights into activation and function of the AMPK. Nat Rev Mol Cell Biol 24:255–272. https://doi.org/10.1038/s41580-022-00547-x

17. Viollet B et al (2003) The AMP-activated protein kinase alpha2 catalytic subunit controls whole-body insulin sensitivity. J Clin Invest 111:91–98. https://doi.org/10.1172/JCI16567
18. Myers RW et al (2017) Systemic pan-AMPK activator MK-8722 improves glucose homeostasis but induces cardiac hypertrophy. Science 357:507–511. https://doi.org/10.1126/science.aah5582
19. Buhl ES et al (2002) Long-term AICAR administration reduces metabolic disturbances and lowers blood pressure in rats displaying features of the insulin resistance syndrome. Diabetes 51:2199–2206. https://doi.org/10.2337/diabetes.51.7.2199
20. Steneberg P et al (2018) PAN-AMPK activator O304 improves glucose homeostasis and microvascular perfusion in mice and type 2 diabetes patients. JCI Insight. https://doi.org/10.1172/jci.insight.99114
21. Cool B et al (2006) Identification and characterization of a small molecule AMPK activator that treats key components of type 2 diabetes and the metabolic syndrome. Cell Metab 3:403–416. https://doi.org/10.1016/j.cmet.2006.05.005
22. Brandt A et al (2019) Metformin attenuates the onset of non-alcoholic fatty liver disease and affects intestinal microbiota and barrier in small intestine. Sci Rep 9:6668. https://doi.org/10.1038/s41598-019-43228-0
23. Dehnavi S et al (2021) Targeting AMPK by Statins: A Potential Therapeutic Approach. Drugs 81:923–933. https://doi.org/10.1007/s40265-021-01510-4
24. Kim SH et al (2017) Ezetimibe ameliorates steatohepatitis via AMP activated protein kinase-TFEB-mediated activation of autophagy and NLRP3 inflammasome inhibition. Autophagy 13:1767–1781. https://doi.org/10.1080/15548627.2017.1356977
25. Jian C et al (2020) Low-dose sorafenib acts as a mitochondrial uncoupler and ameliorates nonalcoholic steatohepatitis. Cell Metab 31:892-908 e811. https://doi.org/10.1016/j.cmet.2020.04.011
26. Boudaba N et al (2018) AMPK re-activation suppresses hepatic steatosis but its downregulation does not promote fatty liver development. EBioMedicine 28:194–209. https://doi.org/10.1016/j.ebiom.2018.01.008
27. Woods A et al (2017) Liver-specific activation of AMPK prevents steatosis on a high-fructose diet. Cell Rep 18:3043–3051. https://doi.org/10.1016/j.celrep.2017.03.011
28. Viollet B et al (2009) AMPK: lessons from transgenic and knockout animals. Front Biosci (Landmark Ed) 14:19–44. https://doi.org/10.2741/3229
29. Zhao P et al (2020) An AMPK-caspase-6 axis controls liver damage in nonalcoholic steatohepatitis. Science 367:652–660. https://doi.org/10.1126/science.aay0542
30. Gluais-Dagorn P et al (2022) Direct AMPK activation corrects NASH in rodents through metabolic effects and direct action on inflammation and fibrogenesis. Hepatol Commun 6:101–119. https://doi.org/10.1002/hep4.1799
31. Schisler JC et al (2013) CHIP protects against cardiac pressure overload through regulation of AMPK. J Clin Invest 123:3588–3599. https://doi.org/10.1172/JCI69080
32. Yang S-J, Jeon S, Baek JW, Lee KM, Park C-S (2021) Regulation of AMPK activity by CRBN is independent of the thalidomide-CRL4CRBN protein degradation axis. Pharmaceuticals. https://doi.org/10.3390/ph14060512
33. Deng M et al (2016) Deubiquitination and activation of AMPK by USP10. Mol Cell 61:614–624. https://doi.org/10.1016/j.molcel.2016.01.010
34. Lee MS et al (2018) Loss of the E3 ubiquitin ligase MKRN1 represses diet-induced metabolic syndrome through AMPK activation. Nat Commun 9:3404. https://doi.org/10.1038/s41467-018-05721-4
35. Ellegaard AM et al (2016) Repurposing cationic amphiphilic antihistamines for cancer treatment. EBioMedicine 9:130–139. https://doi.org/10.1016/j.ebiom.2016.06.013
36. Liang YC et al (2020) The antihistamine deptropine induces hepatoma cell death through blocking autophagosome-lysosome fusion. Cancers (Basel). https://doi.org/10.3390/cancers12061610
37. Chen S, Luster AD (2022) Antihistamines for cancer immunotherapy: more than just treating allergies. Cancer Cell 40:9–11. https://doi.org/10.1016/j.ccell.2021.11.007
38. Li Q et al (2020) Antihistamine drug ebastine inhibits cancer growth by targeting polycomb group protein EZH2. Mol Cancer Ther 19:2023–2033. https://doi.org/10.1158/1535-7163.MCT-20-0250
39. Seo J et al (2023) Ebastine impairs metastatic spread in triple-negative breast cancer by targeting focal adhesion kinase. Cell Mol Life Sci 80:132. https://doi.org/10.1007/s00018-023-04760-5
40. Wen Y, Lambrecht J, Ju C, Tacke F (2021) Hepatic macrophages in liver homeostasis and diseases-diversity, plasticity and therapeutic opportunities. Cell Mol Immunol 18:45–56. https://doi.org/10.1038/s41423-020-00558-8
41. Weston CJ, Zimmermann HW, Adams DH (2019) The role of myeloid-derived cells in the progression of liver disease. Front Immunol 10:893. https://doi.org/10.3389/fimmu.2019.00893
42. Zhang X et al (2020) The role of AMPKalpha2 in the HFD-induced nonalcoholic steatohepatitis. Biochim Biophys Acta Mol Basis Dis 1866:165854. https://doi.org/10.1016/j.bbadis.2020.165854
43. Ronzitti G, Gross DA, Mingozzi F (2020) Human immune responses to adeno-associated virus (AAV) vectors. Front Immunol 11:670. https://doi.org/10.3389/fimmu.2020.00670
44. Issa SS, Shaimardanova AA, Solovyeva VV, Rizvanov AA (2023) Various AAV serotypes and their applications in gene therapy: an overview. Cells. https://doi.org/10.3390/cells12050785
45. Zhao L et al (2024) Recombinant adeno-associated virus 8 vector in gene therapy: opportunities and challenges. Genes Dis 11:283–293. https://doi.org/10.1016/j.gendis.2023.02.010
46. Gardin A, Ronzitti G (2023) Current limitations of gene therapy for rare pediatric diseases: lessons learned from clinical experience with AAV vectors. Arch Pediatr 30:8S46-48S52. https://doi.org/10.1016/S0929-693X(23)00227-0
47. Garcia D et al (2019) Genetic liver-specific AMPK activation protects against diet-induced obesity and NAFLD. Cell Rep 26:192-208 e196. https://doi.org/10.1016/j.celrep.2018.12.036
48. Liang Z et al (2017) AMPK: a novel target for treating hepatic fibrosis. Oncotarget 8:62780–62792. https://doi.org/10.18632/oncotarget.19376
49. Liang J, Mills GB (2013) AMPK: a contextual oncogene or tumor suppressor? Cancer Res 73:2929–2935. https://doi.org/10.1158/0008-5472.CAN-12-3876
50. Vara-Ciruelos D, Dandapani M, Hardie DG (2020) AMP-activated protein kinase: friend or foe in cancer? Annual Rev Cancer Biol 4:1–16. https://doi.org/10.1146/annurev-cancerbio-030419-033619
51. Gao L et al (2021) Proteome analysis of USP7 substrates revealed its role in melanoma through PI3K/Akt/FOXO and AMPK pathways. Front Oncol 11:650165. https://doi.org/10.3389/fonc.2021.650165
52. Price NL et al (2012) SIRT1 is required for AMPK activation and the beneficial effects of resveratrol on mitochondrial function. Cell Metab 15:675–690. https://doi.org/10.1016/j.cmet.2012.04.003
53. Krishnamurthy N, Grimshaw AA, Axson SA, Choe SH, Miller JE (2022) Drug repurposing: a systematic review on root causes, barriers and facilitators. BMC Health Serv Res 22:970. https://doi.org/10.1186/s12913-022-08272-z
54. Tandra G et al (2023) Literature-based discovery predicts antihistamines are a promising repurposed adjuvant therapy for

Parkinson's disease. Int J Mol Sci. https://doi.org/10.3390/ijms241512339
55. Liu X et al (2024) Loratidine is associated with improved prognosis and exerts antineoplastic effects via apoptotic and pyroptotic crosstalk in lung cancer. J Exp Clin Cancer Res 43:5. https://doi.org/10.1186/s13046-023-02914-8
56. Nori M et al (2003) Ebastine inhibits T cell migration, production of Th2-type cytokines and proinflammatory cytokines. Clin Exp Allergy 33:1544–1554. https://doi.org/10.1046/j.1365-2222.2003.01701.x
57. Gray TA, Wilson A, Fortin PJ, Nicholls RD (2006) The putatively functional Mkrn1-p1 pseudogene is neither expressed nor imprinted, nor does it regulate its source gene in trans. Proc Natl Acad Sci U S A 103:12039–12044. https://doi.org/10.1073/pnas.0602216103